Magnetic properties of the multiferroic chromium thio-spinels $CdCr_2S_4$ and $HgCr_2S_4$

Ola Hartmann[1], Georg Michael Kalvius[2], Roger Wäppling[1], Axel Günther[3], Vladimir Tsurkan[3,4,a], Alex Krimmel[3], and Alois Loidl[3]

[1] Department of Physics and Astronomy, Uppsala University, 75121 Uppsala, Sweden
[2] Physics Department, Technische Universität München, 85747 Garching, Germany
[3] Experimental Physics V, Center for Electronic Correlations and Magnetism, Universität Augsburg, 86159 Augsburg, Germany
[4] Institute of Applied Physics, Academy of Sciences, 2028 Chisinau, Republic of Moldova

Abstract. Powder samples of $CdCr_2S_4$ and $HgCr_2S_4$ were investigated with respect to their magnetic behavior using muon spin rotation/relaxation spectroscopy (μSR). In $CdCr_2S_4$, a second order magnetic transition at 83 ± 1 K is confirmed. No influence on the μSR magnetic parameters due to the simultaneous ferroelectric transition was detected. In the limit $T \to 0$, persistent spin fluctuation exists as a consequence of magnetic frustration. The proposed structural transition around 150 K is barely visible in the μSR spectra, indicating that the change in local symmetry is subtle. In $HgCr_2S_4$, we see in zero field at 27 ± 2 K a second order transition from the paramagnetic into a long-range ordered (LRO) magnetic state. This LRO state is characterized in the μSR spectra by a spontaneous spin precession signal. Applications of moderate magnetic fields (up to 450 mT) destroy the precession signal in favor of a rapidly decaying exponential signal. It reflects short-range order (SRO) of strongly correlated dynamic spins. The magnitude of the field required to induce this change is dependent on temperature. The observation of an increase of magnetic spin fluctuations with applied field suggests that spin dynamics play a key role in the field induced changes of the magnetic properties.

1 Introduction

The spinel structure is commonly found in transition metal compounds. In its normal form it has the stoichiometry AB_2X_4 the A-site being tetrahedrally, the B-site octahedrally coordinated by the X ions (O, S, Se) which form a closed packed cubic lattice. Of special interest are the chromium thio-spinels ACr_2S_4. They exhibit a variety of fascinating physical properties like colossal magnetoresistance [1] or, as in the present case, multiferroic behavior [2,3]. These features originate from the subtle interplay between charge, spin, and orbital degrees of freedom and their coupling to the lattice. Furthermore, the spinel B-site is the prototype of a pyrochlore lattice and magnetic ions located on this site are subject to substantial geometric frustration.

$CdCr_2S_4$ is a Mott insulator. The Cd^{2+} ions on the A-site carry neither a magnetic, nor an orbital degree of freedom. The Cr^{3+} ions on the B-site possess half filled t_{2g} shells and are orbitally inactive as well. The spin configuration is $J = S = 3/2$ due to the quenched orbital moments. Ferromagnetism with a Curie temperature of 84 K is well established [4]. T_C is also the ordering temperature for the relaxor ferroelectricity found more recently together with colossal magnetocapacitive behavior [2,5]. These magnetocapacitive effects in $CdCr_2S_4$ have been further elucidated by Sun et al. [6,7]. Ferromagnets showing ferroelectricity are rare. The term 'relaxor ferroelectricity' describes a ferroelectric cluster state with a smeared out polar phase transition. The space group symmetry $Fd\bar{3}m$ of the paramagnetic phase does not allow the existence of a ferroelectric order parameter. Raman spectroscopy [8] suggested the appearance of local lattice distortions around 130 K, causing the loss of inversion symmetry by the off-centering of Cr ions. Previous far-infrared studies [9] found indications for changes in bond nature and charge redistribution. There exists a long-standing discussion about a non-centrosymmetric polar ground state in spinel compounds [10]. These speculations are based on off-center ions in the spinel structure, detected via unusual large Debye-Waller factors [11] and also via the observation of Bragg reflections forbidden in $Fd\bar{3}m$ symmetry (see e.g. [12]). Very recently, an intrinsic large magnetic anisotropy which evolves at low temperatures has been detected in ESR experiments and was found to be compatible with a short-range off-centering of ions [13] and in diffraction experiments using synchrotron radiation [14], the (200) reflection, which is forbidden under $Fd\bar{3}m$ symmetry, appears below 170 K. The intensity of this reflection increases with decreasing temperatures,

[a] e-mail: vladimir.tsurkan@physik.uni-augsburg.de

rises to a plateau between 140 K and 100 K, and finally increases continuously toward $T \to 0$.

$HgCr_2S_4$ has been studied on poly- and single-crystalline samples by numerous methods such as X-ray diffraction, ESR, susceptibility, heat capacity and electrical conductivity. The results of these measurements are summarized in reference [15]. Antiferromagnetic order was found to set in at $T_N = 22$ K despite the fact that on account of a large positive Curie-Weiss temperature $\Theta_{CW} = 142$ K [16] strong ferromagnetic exchange must exist. Neutron diffraction data taken at low temperatures and in zero applied magnetic field suggest a spiral spin configuration [17]. Magnetization and heat capacity data demonstrate that the antiferromagnetic state of $HgCr_2S_4$ is highly sensitive to applied magnetic fields. Already fields of the order of some 100 mT strongly enhance the ferromagnetic correlations and shift the antiferromagnetic state towards soft ferromagnetism. Colossal magnetocapacitance and colossal magnetoresistance was found below ~70 K [3,15].

In this communication, we report the results of a μSR study on $CdCr_2S_4$ and $HgCr_2S_4$. μSR is not directly sensitive to polar properties and the present findings refer mostly to the static and dynamic spin properties of these chromium thio-spinels.

2 Experimental

Polycrystalline material was prepared by solid state reactions from high-purity binary cadmium and mercury sulfides, elemental chromium and sulfur. Single phase quality was confirmed by X-ray diffraction. The powder was pressed between thin aluminized mylar foils and positioned in the center tube of a He-flow cryostat. This sample mount within the He flow ensured proper and uniform temperatures with a stability better than 0.05 K. μSR spectra were taken in zero applied field (ZF) and weak transverse fields (TF = 5 mT) between 2 K and 200 K. For $HgCr_2S_4$ also measurements in longitudinally applied fields (LF) up to 450 mT were carried out in order to study the influences of applied fields. To suppress the background signal from muons stopped outside the sample, the 'VETO' mode [18] was enabled. Time resolution was 1.25 ns and the initial spectrometer dead time ~5 ns.

For details of the μSR technique we refer the reader to treatises available in the literature (see, for example, [19–23]). The quantity measured in a μSR experiment is the time dependence of the count rate asymmetry $A(t)$ between two detectors sensing the positrons emitted in the decay of the muon placed along the muon beam forward and backward with respect to the sample. It can be described by:

$$A(t) = A_0\, G(t), \tag{1}$$

$A(t)$ constitutes the μSR spectrum. Time is counted from the moment of implantation of the muon into the sample. A_0 is the initial (at $t = 0$) asymmetry, typically around 0.2, and $G(t)$ is the μSR spectral function. It contains information on the magnitude, the static distribution and the temporal behavior of the interstitial magnetic field B_μ created by the magnetic moments surrounding the stopped muon and/or by an externally applied field. The measured features of B_μ can be rather directly related to corresponding properties of the magnetic spin system. However, μSR is not able to give direct information on the geometry of the spin lattice, but the μSR spectrum may exclude certain forms of magnetic order suggested for the compound under discussion.

Except for some special cases, the spectral function in ZF for a magnetically LRO powder material is:

$$G^{\mathrm{ZF}}_{\mathrm{LRO}}(t) = \frac{2}{3}\exp(-\lambda_{\mathrm{tr}}t)\,\cos(2\pi\nu_\mu t) + \frac{1}{3}\exp(-\lambda_{\mathrm{lg}}t). \tag{2}$$

The first (transverse) term describes the cases where B_μ is oriented perpendicular to the initial muon spin direction. This induces Larmor precession of the muon spin leading to a damped oscillatory pattern whose frequency is proportional to the mean interstitial field B_μ:

$$\nu_\mu = \gamma_\mu B_\mu \quad \text{with} \quad \gamma_\mu/2\pi = 135\ \mathrm{MHz/T}.$$

Equation (2) describes a sinusoidal oscillation which appears in the case of a commensurate spin structure. For incommensurate structures the cosine term is to be replaced by the zero order Bessel function $J_0(2\pi\nu_\mu t)$. The damping of the oscillatory pattern is given by the transverse relaxation rate λ_{tr} arising mainly from the static distribution (with width $\Delta B_\mu \approx \lambda_{\mathrm{tr}}/\gamma_\mu$) of the interstitial field around its mean value.

The second term refers to the cases where B_μ is oriented parallel to the initial spin direction. Larmor precession is then absent and only dynamic muon spin relaxation exists, which is characterized by the longitudinal relaxation rate λ_{lg}. This rate is directly proportional to the fluctuation rate $1/\tau$ of the magnetic moments generating the interstitial field. The effect of nuclear dipoles is in general insignificant in the presence of LRO magnetism.

In the paramagnetic state, one has for the mean interstitial field $B_\mu = 0$. Under ZF conditions the μSR spectrum shows an exponential decay of asymmetry caused by the rapid fluctuations of the magnetic spins:

$$G^{\mathrm{ZF}}_{\mathrm{par}}(t) = \exp(-\lambda_{\mathrm{par}}t). \tag{3}$$

Of importance is, that the relaxation rate λ_{par} is inversely proportional to the spin fluctuation rate, contrary to λ_{lg} in equation (2). For a normal second-order phase transition, critical slowing down of spin fluctuations will take place when approaching T_C from above, and λ_{par} will rise sharply.

In the preceding discussion of forms of $G(t)$, a unique muon stopping site in the crystalline lattice was assumed, as well as a stationary muon trapped at this site. Muon motion is commonly only seen in very pure elemental metals in the temperature regime used in the present study. Multiple stopping sites are taken care of by using in $G(t)$ sums over expressions like equation (2). The exact position of the stopped muon is a priori not known. Its determination requires usually single crystal data. However, many

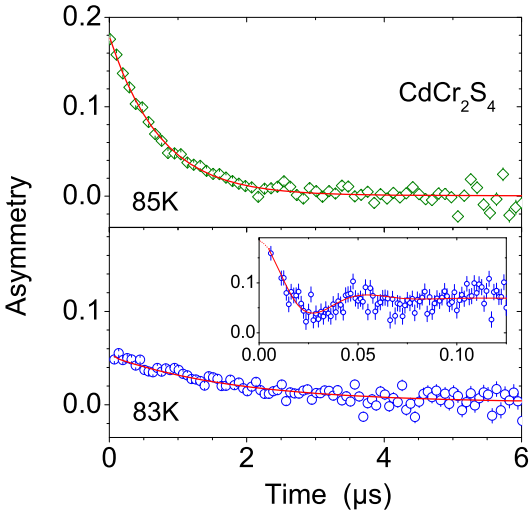

Fig. 1. (top) ZF μSR spectra of $CdCr_2S_4$ at 85 K and (bottom) 83 K. The inset in the bottom panel shows the spectral shape at very early times in high time resolution. The solid lines are least squares fits using the functions given in (top) equation (3) and (bottom) equation (2). Explanation in text.

fundamental conclusions about the internal static and dynamic properties of the magnetic moments can be drawn without exact knowledge of the stopping site.

3 Results

The weak transverse field data taken at various temperatures for both compounds, will not be discussed. They serve to determine the initial asymmetry A_0, are an aid to fix the magnetic transition point, and provide a check for the presence of a background signal. No measurable background signal was found, as is expected when the VETO mode is enabled.

3.1 $CdCr_2S_4$

The ZF spectra of $CdCr_2S_4$ show a distinct sudden change in appearance between 85 K and 83 K as illustrated in Figure 1. At 85 K a simple exponential decay of asymmetry is seen which is the characteristic μSR response for a free paramagnet. This type of spectrum is seen at all temperatures $T \geq 85$ K, except for some more minor details to be discussed further on. The single exponential decay is also proof that all implanted muons rest on a unique interstitial lattice site. The spectrum at 83 K has the expected form if magnetic LRO has set in. The main panel of Figure 1 (bottom) shows an exponential decay, yet with only 1/3 of the initial asymmetry compared to that in the paramagnetic regime. This then is the longitudinal term of equation (2). The inset shows the spontaneous spin precession of the transverse term. It is visible only at very early times (t < 0.1 μs) because of the strong damping of the oscillatory pattern by $\lambda_{\rm tr}$.

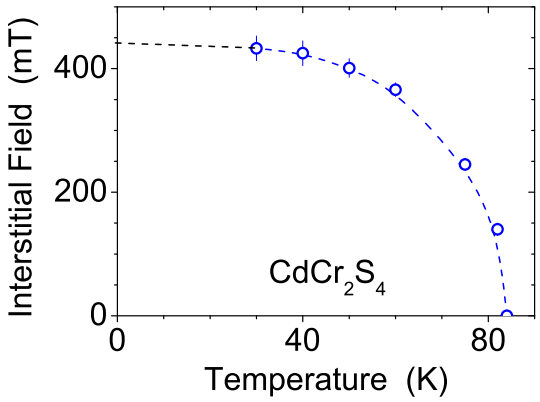

Fig. 2. Temperature dependences of the mean interstitial field B_μ of $CdCr_2S_4$. The dashed line is a guide to the eye.

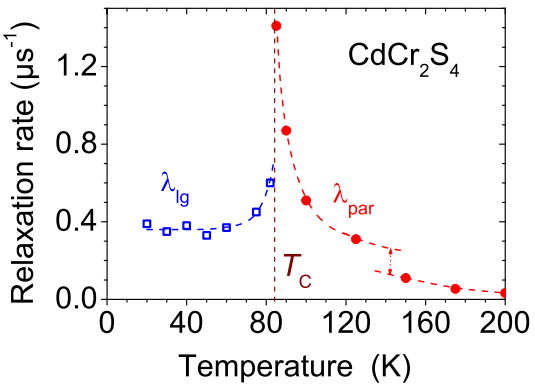

Fig. 3. Temperature dependences of the relaxation rates $\lambda_{\rm lg}$ and $\lambda_{\rm tr}$ in $CdCr_2S_4$. The lines are guides to the eye. For details see text.

The temperature dependence of the interstitial field in the magnetic LRO regime is depicted in Figure 2. It exhibits smooth Brillouin-type behavior, showing that the magnetic spin array is stable, although closeness to an instability in the crystalline lattice has been remarked in reference [15]. The Curie temperature $T_{\rm C} = 84 \pm 1$ K, derived from these data, is in full agreement with published results (e.g. [8]). The saturation field for $T \to 0$ is $B_\mu = 430 \pm 20$ mT. It is comparable to the fields seen in other chromium thio-spinels, e.g. $FeCr_2S_4$ [24]. One obtains for the transverse relaxation rate in the low temperature limit $\lambda_{\rm tr} \approx 125$ μs^{-1}, which corresponds to a field distribution width of $\Delta B_\mu \approx 150$ mT. This width is about 1/3 of the mean field, indicating a reasonably well developed, but not perfect, ferromagnetic spin array.

The dependence on temperature of the longitudinal and paramagnetic relaxation rates $\lambda_{\rm lg}$ and $\lambda_{\rm par}$ is presented in Figure 3. The behavior seen, except for the step in $\lambda_{\rm par}(T)$ around 150 K which will be discussed further below, is characteristic for a second order phase transition at $T_{\rm C}$. Apparent is also that $\lambda_{\rm lg}$ remains at a constant value for $T \to 0$, indicating that the ordered moments do not reach the static limit but display persistent spin fluctuations.

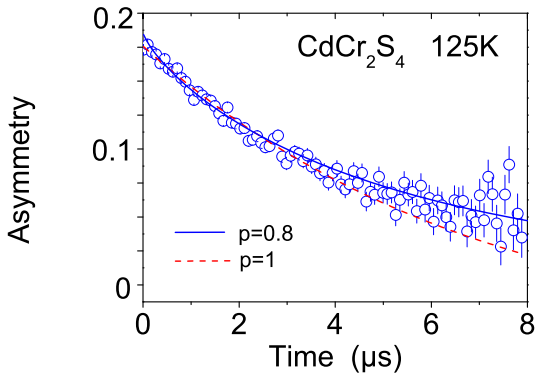

Fig. 4. ZF spectrum of $CdCr_2S_4$ at 125 K with fits to a pure exponential (dashed line) and a power exponential (solid line) relaxation.

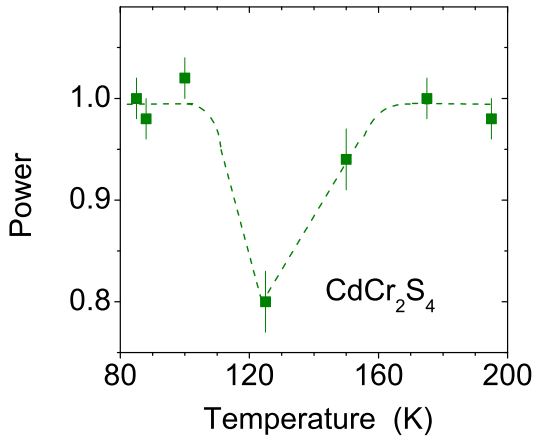

Fig. 5. Temperature dependence of the power p of the power exponential fits to the paramagnetic spectra. The dashed line is a guide to the eye.

Since, the $Fd\bar{3}m$ symmetry of the cubic spinel structure does not allow the formation of a ferroelectric state, some structural transition must occur for $T \geq T_C$. As mentioned, Raman spectroscopy and X-ray diffraction data indicate a lowering of the crystal symmetry in the vicinity of 150 K. The paramagnetic μSR spectra show no dramatic change in this region. One might discern a slight irregularity in the temperature dependence of λ_{par} near 140 K as shown in Figure 3, yet this is at the limit of detectability. Stronger evidence comes from the observation that the ZF spectrum at 125 K cannot be well reproduced by a single purely exponential spin relaxation. As demonstrated in Figure 4, a power-exponential relaxation is a better description of the spectral shape. This means one has to use (see, for example, Sects. 6.4.2.1. and 3.2.2 in Refs. [19] and [20], respectively):

$$G_{par}^{ZF}(t) = \exp\left[-\frac{1}{p}(\lambda_{par}t)^p\right] \qquad (4)$$

instead of equation (3) which corresponds to $p = 1$. Usually, a power-exponential decay signals a distribution of relaxation rates. This may well take place at a structural phase transition. As seen in Figure 5, the deviation from simple exponential decay is most pronounced in the temperature range around 130 K. A structural phase transition is consistent with the μSR data, but the μSR result also stresses that the transition has little influence on the magnetic environment of the stopped muon. Therefore, the change in symmetry must be subtle. As stated already in the introduction, there exists a long-standing debate about a possible phase transition close to 130 K–150 K, where probably the experimental evidence of local lattice distortions, provided by Raman spectroscopy certainly is most striking. Earlier, Göbel [25] reported on an anomalous temperature dependence of the lattice constant and a concomitant broadening of a Bragg reflection. Very recently, Oliveira et al. [26] reported on a dynamic off-centering of Cr ions and a cluster formation accompanied by magneto-electric effects well above the ferromagnetic ordering temperature.

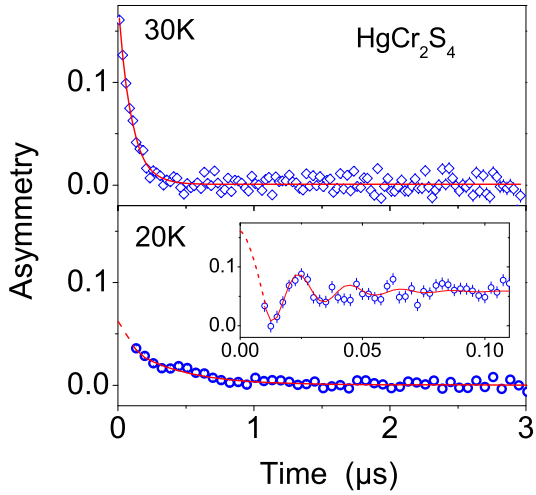

Fig. 6. ZF spectra of $HgCr_2S_4$. Top: at 30 K. The solid line is a fit to a single exponential relaxation. Bottom: at 20 K. The main panel shows a large time range in low-ime resolution, the inset the early times part in high-time resolution. The solid line is a fit to G_{LRO}^{ZF} of equation (2), meaning that the inset shows the transverse term, the main panel the longitudinal term.

3.2 $HgCr_2S_4$

3.2.1 Zero field data

The analysis of the ZF spectra was carried out in the same manner as in the case of $CdCr_2S_4$. As shown in Figure 6, a distinct change in spectral shape takes place between 30 K and 20 K. The spectrum at 30 K features single, purely exponential relaxation, which means that the compound is in the paramagnetic regime. It confirms, in addition, that in $HgCr_2S_4$ as well the stopped muon rests at a single interstitial site. The 20 K spectrum displays spontaneous spin precession and hence reveals that $HgCr_2S_4$ is now in a magnetic LRO state. In general, μSR cannot easily distinguish between ferro and antiferromagnetic order. Furthermore, in the present case the accuracy of the oscillatory pattern is not very high. A more complex fit than a

Table 1. μSR parameters of the ZF spectra of $HgCr_2S_4$ obtained from least squares fits based on the functions given in the last column. The numbers in brackets give the error in the last digits.

T (K)	A_0	$\lambda_{\rm par}$ (μs^{-1})	$\lambda_{\rm lg}$ (μs^{-1})	$\lambda_{\rm tr}$ (μs^{-1})	B_μ (mT)	Function
130	0.20	0.07(5)	–	–	–	$G^{\rm ZF}_{\rm par}$
75	0.21	0.25(1)	–	–	–	$G^{\rm ZF}_{\rm par}$
50	0.20)	0.9(2)	–	–	–	$G^{\rm ZF}_{\rm LRO}$
30	0.19	13(4)	–	–	–	$G^{\rm ZF}_{\rm LRO}$
20	0.17	–	2.1(2)	49(2)	350(15)	$G^{\rm ZF}_{\rm LRO}$
10	0.17	–	0.1(3)	68(3)	400(15)	$G^{\rm ZF}_{\rm LRO}$
1.8	0.18	–	0.06(4)	91(4)	425(25)	$G^{\rm ZF}_{\rm LRO}$

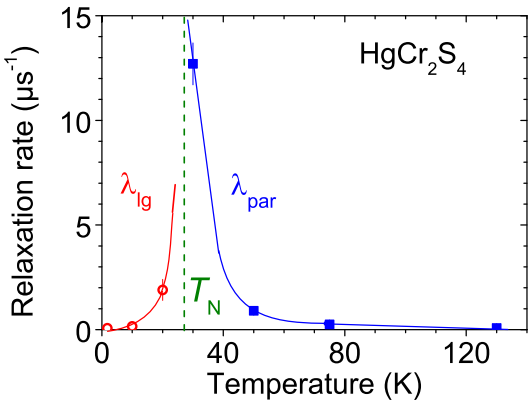

Fig. 7. Temperature dependences of the relaxation rates $\lambda_{\rm lg}$ and $\lambda_{\rm par}$ in $HgCr_2S_4$. The lines are guides to the eye. From the plot one derives $T_{\rm N} = 27 \pm 2$ K.

single cosine oscillation is not indicated. Neutron diffraction data are interpreted in terms of an antiferromagnetic spiral spin structure [17].

The relevant parameters of the ZF spectra of $HgCr_2S_4$ are summarized in Table 1. The saturation ($T \to 0$) field of $B_\mu = 425 \pm 25$ mT is about the same as in $CdCr_2S_4$. The transverse relaxation rate in the low temperature limit is in $HgCr_2S_4$ slightly smaller than in $CdCr_2S_4$. The LRO spin state is well developed under zero field conditions.

Figure 7 depicts the temperature dependences of the two relaxation rates $\lambda_{\rm lg}$ ($T < T_{\rm N}$) and $\lambda_{\rm par}$ ($T > T_{\rm N}$). From the plot one deduces a transition temperature $T_{\rm N} = 27 \pm 2$ K. This value is slightly higher than $T_{\rm N} = 22$ K given in reference [9]. The variation with temperature of the relaxation rates shown in Figure 7 is consistent with $T_{\rm N}$ being a second order phase transition like in $CdCr_2S_4$. Different to $CdCr_2S_4$ is the absence of persistent spin fluctuations. The ordered moments in $HgCr_2S_4$ reach the static limit for $T \to 0$.

3.2.2 Longitudinal field data

Previous bulk magnetic data established a high sensitivity of the antiferromagnetic groundstate of $HgCr_2S_4$ to applied external magnetic fields. To gain further information on this most interesting behavior, we have recorded longitudinal field (LF = 100, 300, and 450 mT) spectra at various temperatures below and above $T_{\rm N}$ in zero field (the term 'longitudinal field' means that the field is applied along the muon beam axis i.e. along the initial direction of the muon spin). It, thus, will not induce Larmor precession. However, since powder samples were used, the direction of the applied field is random with respect to crystalline symmetry axes.

The application of stronger longitudinal fields affects the response of the μSR spectrometer. The main reasons are the sensitivity to magnetic fields of the detectors for the positrons emitted in the muon decay and the bending of the flight path from the sample to the detectors of the emitted positrons. These effects were studied in dummy runs. It was found that up to 450 mT the influence on spectral shape was not severe and could be taken care of in the data analysis. We have avoided to go to higher fields since then the situation becomes more complex.

The ZF and LF spectra taken at different temperatures up to 50 K (i.e. above $T_{\rm N}$ in ZF) are shown in Figure 8. They are plotted in low-time resolution and only the longitudinal term (with $A_0/3$ initial asymmetry) is seen as long as a magnetic LRO state is present.

At 1.8 K (Fig. 8a), no influence of the applied fields on spectral shape is noticeable. The longitudinal relaxation rate remains constant within the limits of error at $\sim 0.06\,\mu s^{-1}$, that is, in the static limit. A spontaneous spin precession is visible only at early times in high time resolution spectra and is similar to that in the ZF spectrum (see Fig. 6).

At 10 K (Fig. 8b), the ZF, the $B_{\rm LF} = 100$ and 300 mT spectra still show only the longitudinal term with $A_0/3$ initial asymmetry and, thus, reflect the LRO state. The difference in shape between the ZF and the $B_{\rm LF} = 300$ mT spectra demonstrates that here, in contrast to the situation at 1.8 K, the longitudinal relaxation rate increases with field (from 0.1 μs^{-1} to 0.3 μs^{-1}). Clearly, the applied field increases the fluctuations of the ordered moments. At $B_{\rm LF} = 450$ mT, the spectrum alters its appearance markedly. Now, only a fast relaxing spectrum with $\lambda = 0.50\,\mu s^{-1}$ having the total initial asymmetry $A_0 = 0.17$ is seen without a spin precession signal being present. The magnetic LRO has been destroyed by the applied field. The spectral shape seen is indicative of a dynamic SRO spin arrangement. According to magnetization data [15], the short-range correlations are ferromagnetic.

At 20 K (Fig. 8c), the transition from LRO to SRO occurs already between $B_{\rm LF} = 100$ mT and $B_{\rm LF} = 300$ mT. In the LRO regime, the longitudinal relaxation rate increases distinctly again when going from ZF to $B_{\rm LF} = 100$ mT, indicating here also a speed up of spin dynamics. In the SRO regime the relaxation decreases with field. One must, however, realize that in the LRO regime one is in the slow fluctuation limit (where $\lambda_{\rm lg}$ is proportional to $1/\tau$), while in the SRO state one is in the fast fluctuation limit where $\lambda_{\rm SRO}$ is proportional to τ.

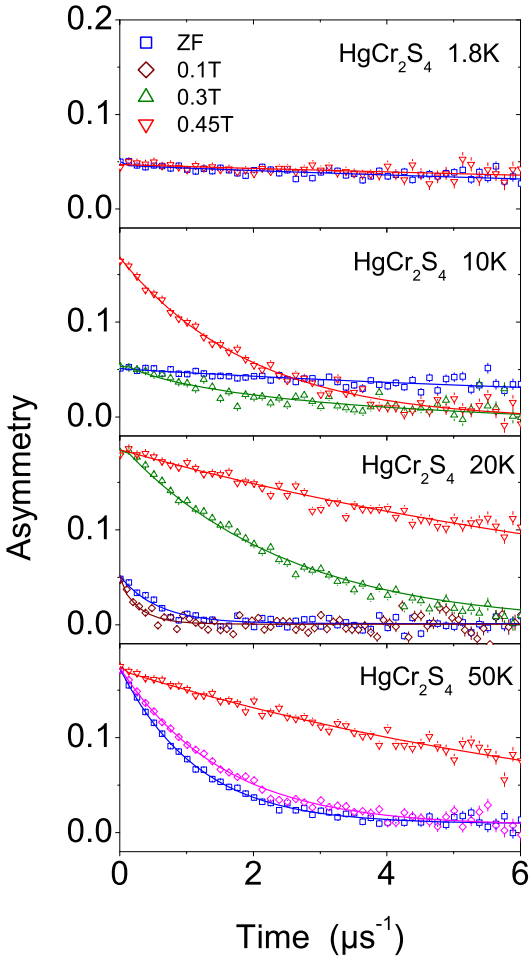

Fig. 8. ZF and LF spectra of $HgCr_2S_4$ between 1.8 K and 50 K. The solid lines are least squares fits explained in text. For clarity only the ZF and $B_{LF} = 450$ mT spectra are plotted at 1.8 K. At 10 K, the $B_{LF} = 100$ mT spectrum has been omitted.

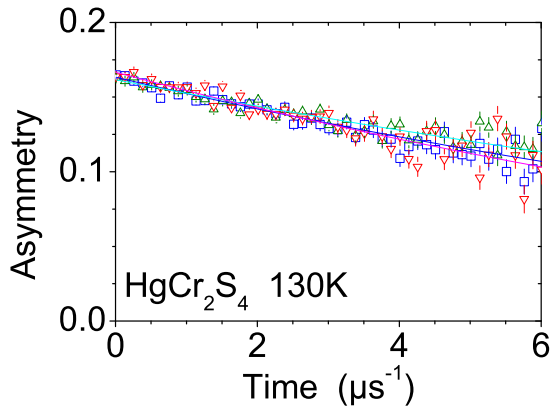

Fig. 9. ZF and LF spectra of $HgCr_2S_4$ at 130 K. The symbols are the same as used in Figure 8. The $B_{LF} = 100$ mT spectrum has been omitted for clarity.

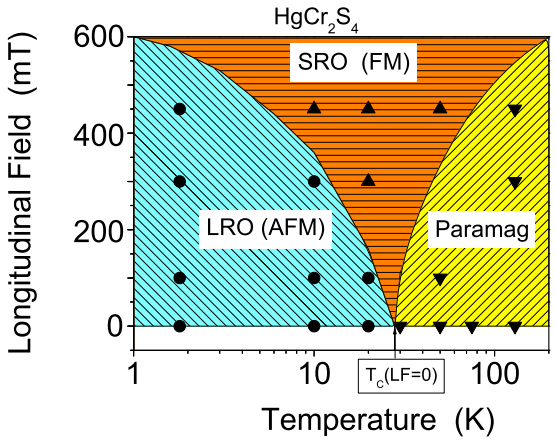

Fig. 10. Schematic B–T phase diagram of $HgCr_2S_4$ derived from the ZF and LF μSR spectra.

Hence, the observation of slower relaxation in the SRO state is due to an increase of spin fluctuation with field.

At 50 K (Fig. 8d), $HgCr_2S_4$ is well in the paramagnetic state. Applying a longitudinal field of 100 mT causes little change in spectral shape except for a weak decrease of the relaxation rate λ_{par}. This is a well-known phenomena in a paramagnet, discussed initially for NMR [27]. The effect is described by the equation:

$$\lambda_{par}(B_{LF}) = \frac{\lambda_{par}(B_{ZF})}{1 + (\gamma_\mu B_{LF}\tau)^2}. \qquad (5)$$

Putting into equation (5), the measured value of the ratio

$$\lambda_{par}(0.1\mathrm{T})/\lambda_{par}(ZF) = 0.77$$

leads to $1/\tau \approx 200$ MHz, a fairly slow paramagnetic relaxation rate. Clearly, spin-spin correlations are still rather strong. Increasing the longitudinal field to 450 mT should only cause a moderate further reduction of the relaxation rate on the basis of equation (5). In contrast, however, the spectrum depicted in Figure 8d shows that the relaxation rate has become significantly smaller. Based on this consideration, we interpret the spectrum at $B_{LF} = 450$ mT as indicative for a re-entrance into the SRO state.

Finally, we have measured the influence of longitudinal fields at 130 K where $HgCr_2S_4$ is deep inside its paramagnetic regime. The spectra are depicted in Figure 9. As expected, the influence of the applied fields is barely measurable meaning that the spin fluctuation rate has vastly increased. Using once more equation (5) gives a fluctuation rate of $1/\tau > 5$ GHz, a value characteristic for a free paramagnet with very weak spin-spin correlations.

From the findings discussed above one is able to derive a schematic B–T phase diagram presented in Figure 10. Interestingly, at zero external magnetic fields this is a transition from an antiferromagnetic into a paramagnetic state. However, already at low fields the system is dominated by ferromagnetic fluctuations.

4 Summary

$CdCr_2S_4$: the μSR results are largely in agreement with earlier bulk magnetic measurements, especially with

respect to the magnetic Curie point $T_C = 84 \pm 1$ K and the pure second order nature of the transition. No influence of the simultaneous occurring ferroelectric transition on the temperature dependences of the interstitial field and the spin fluctuation rate is noticeable. The field at the muon site (∼425 mT) is similar to that found in other chromium thio-spinels, indicating that the atomic structure of the Cr^{3+} ions is similar in the different thio-spinel compounds.

The proposed, and for the formation of a ferroelectric state necessary, structural transition around 150 K is only weakly discernible in the μSR spectra. In fact, from the μSR data alone one could not safely claim its existence. The weak variation in shape of the μSR spectra around the proposed transition indicates that the lattice distortion must be subtle. The suggested off-centering of the Cr ions [8] is fully consistent with the μSR findings.

The fluctuation rate $1/\tau$ of the Cr^{3+} ordered magnetic moments remains at a steady, albeit small, value at low temperatures, i.e. the fully static limit is not reached in the limit $T \rightarrow 0$. These 'persistent spin fluctuations' are typical in magnetically frustrated systems [28–30] and most easily detected by μSR.

$HgCr_2S_4$: the μSR results in zero field are basically similar to those seen in $CdCr_2S_4$. The second order transition from paramagnetism to LRO is found to occur at $T_N = 27 \pm 2$ K. This value is close to the results of recent bulk measurements [15], but also refutes older measurements of $T_N = 36$ K [16]. The interpretation of susceptibility and magnetization measurements in $HgCr_2S_4$ are complicated and sometimes misleading, as at elevated temperatures the system is dominated by ferromagnetic fluctuations and is very close to ferromagnetic order, but finally orders antiferromagnetically at 27 K. This has been extensively documented in reference [15]. Zero-field mSR experiments are ideally suited to verify this behavior. The exact nature of the LRO state cannot be derived from the μSR data. But again the LRO spin array is well developed with little local distortions. The magnetic field at the muon site is about the same as in $CdCr_2S_4$, showing that no significant change in magnitude of the Cr^{3+} ordered moment occurs when changing the anion from Cd to Hg, despite the reduction of the ordered moment when compared to the free ion value.

The changes in magnetic properties as manifested in the μSR spectra taken under externally applied, comparatively low, magnetic fields (≤450 mT) are of particular interest since they can be compared with those used in the bulk magnetic measurements [15]. At low temperature (1.8 K), where the ordered moments are in the static limit, the applied fields have essentially no influence on the properties of the LRO state, as reflected in the unchanged μSR spectra. At more elevated temperatures, but still below T_N in zero field (i.e. at 10 K and 20 K), the LRO state disappears at certain field magnitudes which depend on temperature. From the shape of its μSR spectra one concludes that the newly formed state is best described as a dynamic short-range ordered spin state. Significant is also the observation, that in the LRO state (i.e. before the SRO state is formed) the fluctuation rate of the ordered moment is enhanced by the applied field. At 50 K, where in zero and low applied fields the compound is paramagnetic, although with marked spin-spin correlations, the spectrum at 450 mT suggests a re-entry into the SRO state. At 130 K, $HgCr_2S_4$ is in the free paramagnetic state where spin-spin correlations are very low.

Frustration obviously is not prominent in $HgCr_2S_4$, from a μSR point of view established by the absence of persistent spin fluctuations. It is, thus, unlikely that frustration is the driving force for the peculiar magnetic behavior of $HgCr_2S_4$ under applied field. This was also discussed in some detail in reference [15]. Remarkable is that, according to the μSR data, the LRO magnetic spins increase their fluctuation rate under applied field, once the the static limit have been left. The increased spin fluctuations under applied field and with them the reduction of correlation length makes the LRO state unstable, leading finally to the highly dynamic SRO state.

The μSR findings on the field dependence of the magnetism of $HgCr_2S_4$ at different temperatures have been summarized in a B–T phase diagram. It shows three magnetic regions to exist:

1) a LRO state (supposedly an antiferromagnetic spiral structure) in the low temperature-low field regimes;
2) a SRO state at more elevated temperatures and higher fields;
3) a paramagnetic state at even higher temperatures.

In the low temperature limit, the LRO state is stable, while in the high temperature limit, the paramagnetic state exists at all fields applied ($B \leq 450$ mT). It is also worth mentioning that in ZF the direct transition from the antiferromagnetic state to the paramagnetic state via a standard second order transition is possible, while even in low applied magnetic fields (e.g. 300 mT) the paramagnetic state is reached only by transgressing through a ferromagnetically short-range ordered state.

The experiments were carried out using the μSR spectrometers DOLLY and GPS at the Swiss Muon Source, Paul Scherrer Institute (PSI), Villigen-AG, Switzerland. We are indebted to H. Luetgens and R. Scheuermann for continuous support during the experiments. One of us (GMK) is indebted to A. Yaouanc for helpful discussions. The work was supported in part by the Deutsche Forschungsgemeinschaft via TRR88 (Augsburg-Munich) and via the Research Unit FOR960.

References

1. A.P. Ramirez, R.J. Cava, J. Krajewski, Nature **386**, 156 (1997)
2. J. Hemberger, P. Lunkenheimer, R. Fichtl, H.-A. Krug von Nidda, V. Tsurkan, A. Loidl, Nature **434**, 364 (2005)
3. S. Weber, P. Lunkenheimer, R. Fichtl, J. Hemberger, V. Tsurkan, A. Loidl, Phys. Rev. Lett. **96**, 157202 (2006)
4. P.K. Baltzer, H.W. Lehmann, M. Robbins, Phys. Rev. Lett. **15**, 493 (1965)

5. P. Lunkenheimer, R. Fichtl, J. Hemberger, V. Tsurkan, A. Loidl, Phys. Rev. B **72**, 060103(R) (2005)
6. C.P. Sun, C.C. Lin, J.L. Her, C.J. Ho, S. Taran, H. Berger, B.K. Chaudhuri, H.D. Yang, Phys. Rev. B **79**, 214116 (2009)
7. C.P. Sun, C.L. Huang, C.C. Lin, J.L. Her, C.J. Ho, J.-Y. Lin, H. Berger, H.D. Yang, J. Appl. Phys. **96**, 122109 (2010)
8. V. Gnezdilov, P. Lemmens, Y.G. Pashkevich, Ch. Payen, K.Y. Choi, J. Hemberger, A. Loidl, V. Tsurkan, Phys. Rev. B **84**, 045106 (2011)
9. T. Rudolf, Ch. Kant, J. Hemberger, V. Tsurkan, A. Loidl, Phys. Rev. B **76**, 174307 (2007)
10. N.W. Grimes, J. Phys. C **6**, L78 (1973)
11. N.W. Grimes, Philos. Mag. **26**, 1217 (1972)
12. A.H. Heuer, T.E. Mitchell, J. Phys. C **8**, L541 (1975)
13. D. Ehlers, V. Tsurkan, H.-A. Krug von Nidda, A. Loidl, Phys. Rev. B **86**, 174423 (2012)
14. A. Krimmel, unpublished
15. V. Tsurkan, J. Hemberger, A. Krimmel, H.-A. Krug von Nidda, P. Lunkenheimer, S. Weber, V. Zestrea, A. Loidl, Phys. Rev. B **73**, 224442 (2006)
16. P.K. Baltzer, P.J. Wojtowicz, M. Robbins, E. Lopatin, Phys. Rev. **151**, 367 (1966)
17. J.M. Hasting, L.M. Corliss, J. Phys. Chem. Solids **29**, 9 (1968)
18. D.J. Arsenau, B. Hitti, S.R. Kreitzmann, E. Whidden, Hyperfine Interactions **106**, 277 (1997)
19. A. Yaouanc, P. Dalmas de Réotier, *Muon Spin Rotation, Relaxation, and Resonance* (Oxford University Press, Oxford, 2011)
20. G.M. Kalvius, D.R. Noakes, O. Hartmann, in *Handbook on the Physics and Chemistry of Rare Earth*, edited by K.A. Gschneidner et al. (Elsevier Science, Amsterdam, 2001), Vol. 32, p. 55ff
21. *Muon Science*, edited by S.L. Lee, S.H. Kilcoyne, R. Cywinski (IOP, London, 1999)
22. E. Karlsson, *Solid State Phenomena as seen by Muons, Protons and Excited Nuclei* (Oxford University Press, Oxford, 1995)
23. A. Schenck, *Muon Spin Rotation Spectroscopy* (Adam Hilger, Bristol, 1985)
24. G.M. Kalvius, A. Krimmel, R. Wäppling, O. Hartmann, F.J. Litterst, F.E. Wagner, V. Tsurkan, A. Loidl, J. Phys.: Condens. Matter **22**, 052205 (2010)
25. H. Göbel, J. Magn. Magn. Mater. **3**, 143 (1976)
26. G.N.P. Oliveira, A.M. Pereira, A.M.L. Lopes, J.S. Amaral, A.M. dos Santos, Y. Ren, T.M. Mendonça, C.T. Sousa, V.S. Amaral, J.G. Correia, J.P. Araújo, Phys. Rev. B **86**, 224418 (2012)
27. C.P. Slichter, *Principles of Magnetic Resonance* (Springer, Berlin/New York, 1978), Chap. 5
28. A. Yaouanc, P. Dalmas de Réotier, P. Bonville, J.A. Hodges, P.C.M. Gubbens, C.T. Kaiser, S. Sakarya, Physica B **326**, 456 (2003)
29. G.M. Kalvius, D. Noakes, R. Wäppling, G. Grosse, W. Schäfer, W. Kockelmann, J.K. Yakinthos, P.A. Kotsanides, Physica B **326**, 465 (2003)
30. G.M. Luke, A. Keren, K. Kojiima, L.P. Le, W.D. Wu, U.J. Uemura, G.M. Kalvius, A. Kratzer, G. Nakamoto, T. Takabatake, M. Ishikawa, Physica B **206-207**, 222 (1995)